ARTICLES

Structure of the outer membrane complex of a type IV secretion system

Vidya Chandran[1]*, Rémi Fronzes[1]*, Stéphane Duquerroy[2,3], Nora Cronin[1], Jorge Navaza[4] & Gabriel Waksman[1]

Type IV secretion systems are secretion nanomachines spanning the two membranes of Gram-negative bacteria. Three proteins, VirB7, VirB9 and VirB10, assemble into a 1.05 megadalton (MDa) core spanning the inner and outer membranes. This core consists of 14 copies of each of the proteins and forms two layers, the I and O layers, inserting in the inner and outer membrane, respectively. Here we present the crystal structure of a ~0.6 MDa outer-membrane complex containing the entire O layer. This structure is the largest determined for an outer-membrane channel and is unprecedented in being composed of three proteins. Unexpectedly, this structure identifies VirB10 as the outer-membrane channel with a unique hydrophobic double-helical transmembrane region. This structure establishes VirB10 as the only known protein crossing both membranes of Gram-negative bacteria. Comparison of the cryo-electron microscopy (cryo-EM) and crystallographic structures points to conformational changes regulating channel opening and closing.

Type IV secretion (T4S) systems are used by Gram-negative bacteria in a variety of processes, ranging from the delivery of virulence factors into eukaryotic cells to conjugative transfer of genetic material and the uptake or release of DNA[1–3]. In *Helicobacter pylori*, *Brucella suis* and *Legionella pneumophila*, T4S systems mediate the injection of virulence proteins into mammalian host cells to cause gastric ulcers, brucellosis, or Legionnaire's disease, respectively[4,5]. In *Agrobacterium tumefaciens*, the VirB/D T4S system delivers oncogenic DNA and proteins into plant cells[2,6], and *Bordetella pertussis* uses a T4S system to secrete the pertussis toxin into the extracellular milieu[7]. Conjugation promotes bacterial genome plasticity and the adaptive response of bacteria to changes in the environment, contributing to the spread of antibiotic-resistance genes among pathogenic bacteria[8].

Although variations exist, many of the T4S systems found in Gram-negative bacteria are similar to the *A. tumefaciens* VirB/D T4S system, which comprises 12 proteins named VirB1 to VirB11 and VirD4[2]. In general (but not always), T4S systems include an extracellular pilus composed of a major (VirB2) and a minor (VirB5) subunit[9]. Three ATPases located at the inner membrane, VirB4, VirB11, and VirD4, power substrate secretion and possibly assist in the assembly of the system[2,10]. The inner-membrane channel is thought to be composed of the polytopic membrane protein VirB6 and the bitopic membrane proteins VirB8 and VirB10[2]. At the outer membrane, the composition of the pore that allows the substrate to reach the extracellular milieu is unknown. VirB9 in complex with the short lipoprotein VirB7 could be part of this structure. A region of the carboxy (C)-terminal domain of VirB9 was shown to be surface-exposed[11]. However, no transmembrane region could be found or predicted in both proteins.

Recently, the cryo-EM structure of the core complex of the T4S system encoded by the conjugative plasmid pKM101 showed that T4S systems consist of a 1.05 MDa core spanning the inner and outer membranes of Gram-negative bacteria[12]. This core, extracted pre-assembled from the membranes using detergents, is composed of two layers, the O and I layers, and is formed by 14 copies of three proteins, the homologues of the VirB7, VirB9 and VirB10 proteins, termed TraN, TraO and TraF, respectively. Here we present the crystal structure of the T4S system outer-membrane complex, containing the entire O layer.

General architecture of the complex

The T4S system outer-membrane complex was obtained from chymotryptic cleavage of the T4S system core, crystallized and its structure solved as described in the Methods (see also Supplementary Table 1 and Supplementary Fig. 1). This 590 kDa complex contains 14 copies each of the C-terminal domain of TraF ($TraF_{CT}$; residues 160–386), the C-terminal domain of TraO ($TraO_{CT}$; residues 160–294) and the full-length TraN (Supplementary Fig. 1a). The hetero-tetradecameric structure of the T4S system outer-membrane complex has an elegant architecture with 14-fold symmetry (Fig. 1a). In the cryo-EM work, the O layer was described as containing two parts: the main body and the cap. In the crystal structure, the cap is made of a hydrophobic ring of two-helix bundles defining a 32 Å channel (Fig. 1a, b). These helices are made of residues 307–355 of $TraF_{CT}$. The main body is made of the rest of $TraF_{CT}$, $TraO_{CT}$ and TraN. It has a 172 Å diameter (Fig. 1b). When the complex is viewed from the top, that is, from the extracellular milieu (Supplementary Fig. 2a), $TraF_{CT}$ forms an inner ring surrounded by the $TraO_{CT}$–TraN complex. The TraN protein forms spokes radially crossing the entire assembly (Supplementary Fig. 2a, b). When the complex is viewed from the bottom, that is, from the periplasm (Supplementary Fig. 2c), the structure is primarily made of $TraF_{CT}$. A cut-away view of the structure (Fig. 1b) shows that TraF forms the entirety of the inner wall of the structure, establishing VirB10 homologues as T4S system outer-membrane channel proteins, an unexpected result as VirB10 homologues have never been suspected to form the outer-membrane channel of T4S systems. VirB10 homologues are also found in the inner-membrane fraction owing to the presence of a transmembrane helix at the amino (N) terminus of the protein[13]. Thus, VirB10 is the only protein known to insert in both inner and outer membranes of Gram-negative bacteria.

[1]Institute of Structural and Molecular Biology, University College London and Birkbeck College, Malet Street, London WC1E 7HX, UK. [2]Institut Pasteur, Unité de Virologie Structurale, Virology Department and CNRS URA 3015, Paris, 25–28 Rue du Dr Roux, F-75724 Paris, France. [3]Université Paris-Sud, F-91405 Orsay, France. [4]Laboratoire de Microscopie Electronique, Institut de Biologie Structurale J.P. Ebel, 41 rue Jules Horowitz, F-38027 Grenoble Cedex 1, France.
*These authors contributed equally to this work.

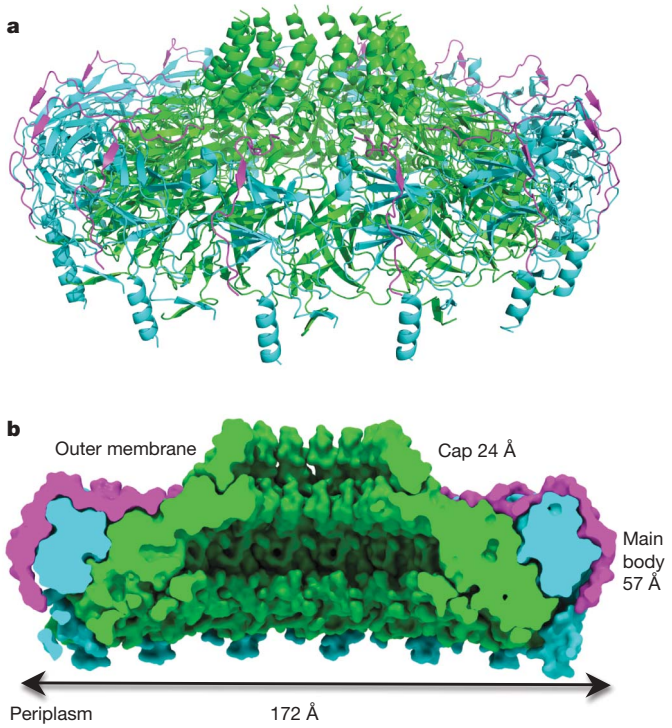

Figure 1 | The T4S system outer-membrane complex. Ribbon diagram (**a**) and space-filling cut-away (**b**) of the tetradecameric complex. $TraF_{CT}$, $TraO_{CT}$ and TraN subunits are colour-coded green, cyan and magenta, respectively. In **b**, dimensions and labelling of the various parts of the complex are provided.

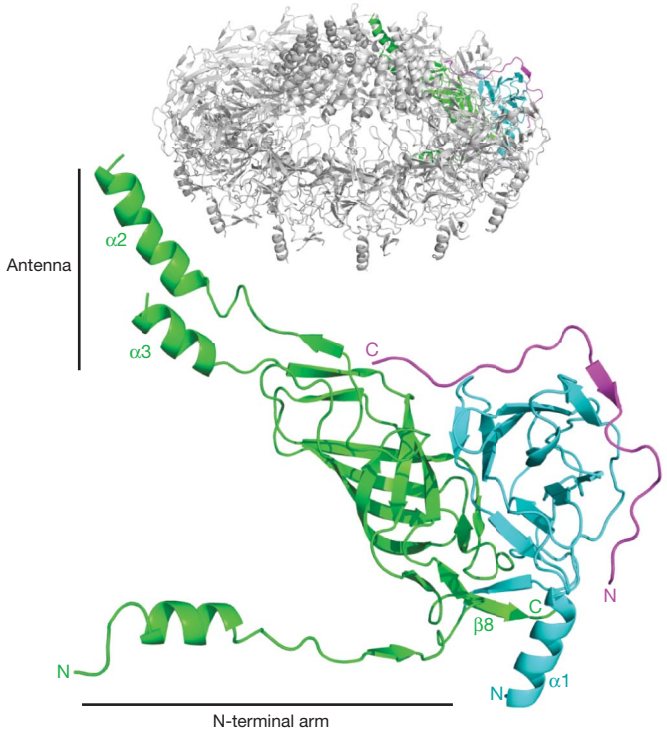

Figure 2 | Ribbon diagram of the heterotrimer unit. Structures mentioned in the main text are indicated. The insert locates the shown heterotrimer within the tetradecameric structure. A stereo version of this figure with full secondary structure labelling is provided in Supplementary Fig. 2d.

Structure of the heterotrimer unit

A unique feature of the T4S system outer-membrane complex is that it is made of three proteins (instead of one for all outer-membrane structures previously determined), all three being indispensable for complex assembly and channel formation[12]. The heterotrimer formed by $TraF_{CT}$, $TraO_{CT}$ and TraN is shown in Fig. 2 (see also Supplementary Fig. 2d). The interfaces between $TraF_{CT}$ and $TraO_{CT}$ and between $TraO_{CT}$ and TraN bury 2861 $Å^2$ and 2024 $Å^2$ of surface area, respectively. TraN does not interact with $TraF_{CT}$ in the heterotrimer. The core structure of the $TraO_{CT}$–TraN complex bound to $TraF_{CT}$ is similar to the previously determined NMR structure of the $TraO_{CT}$–TraN complex alone (Fig. 2; details in Supplementary Information and Supplementary Fig. 3a, b)[11]. However, there are also important differences. First, in $TraO_{CT}$ bound to $TraF_{CT}$, residues 162–173 at the N terminus form the α1 helix (Fig. 2). In the tetradecamer, 14 α1 helices form 14 pillars onto which the entire complex sits on the I layer (Fig. 1a). Second, at the C terminus, residues 286–289 have become ordered in $TraO_{CT}$ bound to $TraF_{CT}$ to form the β10 strand. β10 of $TraO_{CT}$ is part of the $TraF_{CT}$–$TraO_{CT}$ interface as it forms a two-stranded β-sheet with β8 of $TraF_{CT}$ (see Fig. 2 where, for clarity, only β8 of $TraF_{CT}$ is indicated). In TraN, sequences at the N (residues 15–25) and C (residues 37–42) termini have become ordered in the heterotrimer. Remarkably, TraN almost entirely wraps around $TraO_{CT}$, forming an interface with $TraO_{CT}$ that is much more extensive than that observed in the NMR structure (see details in Supplementary Information and Supplementary Fig. 3c).

The structure of the apo form of the C-terminal domain of ComB10 ($ComB10_{CT}$), a TraF/VirB10 homologue, has been solved[14]. It consists of an atypical β-barrel flanked by an α-helix, onto which an 'antenna'-like structure is mounted (Supplementary Fig. 3d). $TraF_{CT}$ in the heterotrimer differs from $ComB10_{CT}$ in three major ways: (1) the flanking helix of $ComB10_{CT}$ is missing in $TraF_{CT}$; (2) the antenna structure of $TraF_{CT}$ is more extended; and (3) the N terminus of $TraF_{CT}$ forms an extended N-terminal arm (or lever arm; residues 171–199) that projects out to interact with three consecutive neighbouring heterotrimers in the tetradecameric assembly (Figs 2 and 3, and Supplementary Figs 3e and 4).

Tetradecameric assembly

The interactions between heterotrimers in the tetradecameric outer-membrane complex are extensive (details are provided in Supplementary Figs 4–7 and Supplementary Information). To help orientate the reader, a consistent colour scheme summarized in Fig. 3a, e is provided, in which the TraF/VirB10, TraO/VirB9 and TraN/VirB7 subunits are numbered clockwise F1–F14, O1–O14 and N1–N14, respectively.

Of the 13,000 $Å^2$ of total surface area of $TraF_{CT}$, 11% is involved in intra-heterotrimeric interactions and 51.5% is involved in interactions between heterotrimers (Supplementary Fig. 8a, b). $TraF_{CT}$ of one heterotrimer (for example F1 in green in Fig. 3a, b) interacts not only with two adjacent $TraF_{CT}$ subunits (F2 and F14), but also, because of the long N-terminal lever arm, with four neighbouring $TraF_{CT}$ subunits located further afield (F3, F4 on one side and F13 and F12 on the other; Fig. 3b). In addition, $TraF_{CT}$ interacts with the $TraO_{CT}$ and TraN subunits of an adjacent heterotrimer (O14 and N14 in Fig. 3a)

The interface between $TraF_{CT}$ subunits includes 2320 $Å^2$ of surface area and is described in detail in the Supplementary Information and in Supplementary Fig. 6. Strand additions and numerous loop–loop interactions constitute important parts of the interface. Yet, its most notable feature is the N-terminal lever arm of the $TraF_{CT}$ subunit, which makes its own extensive interaction network. The arm of subunit FX ($1 \leq X \leq 14$) interacts with the subunit F$X+1$, F$X+2$ and F$X+3$ (for example, see Fig. 3b, c where the F1 lever arm interacts with subunits F2, F3 and F4). FX − F$X+1$, FX − F$X+2$ and FX − F$X+3$ contacts involve residues in the β_n1 strand, the $\beta_n1 - \alpha_n1$ linker, and α_n1 helix of the FX subunit lever arm, respectively (Fig. 3c and Supplementary Fig. 6c, d). Overall, the N-terminal lever arms form a continuous inner shelf at the base of the outer-membrane complex (Fig. 3d).

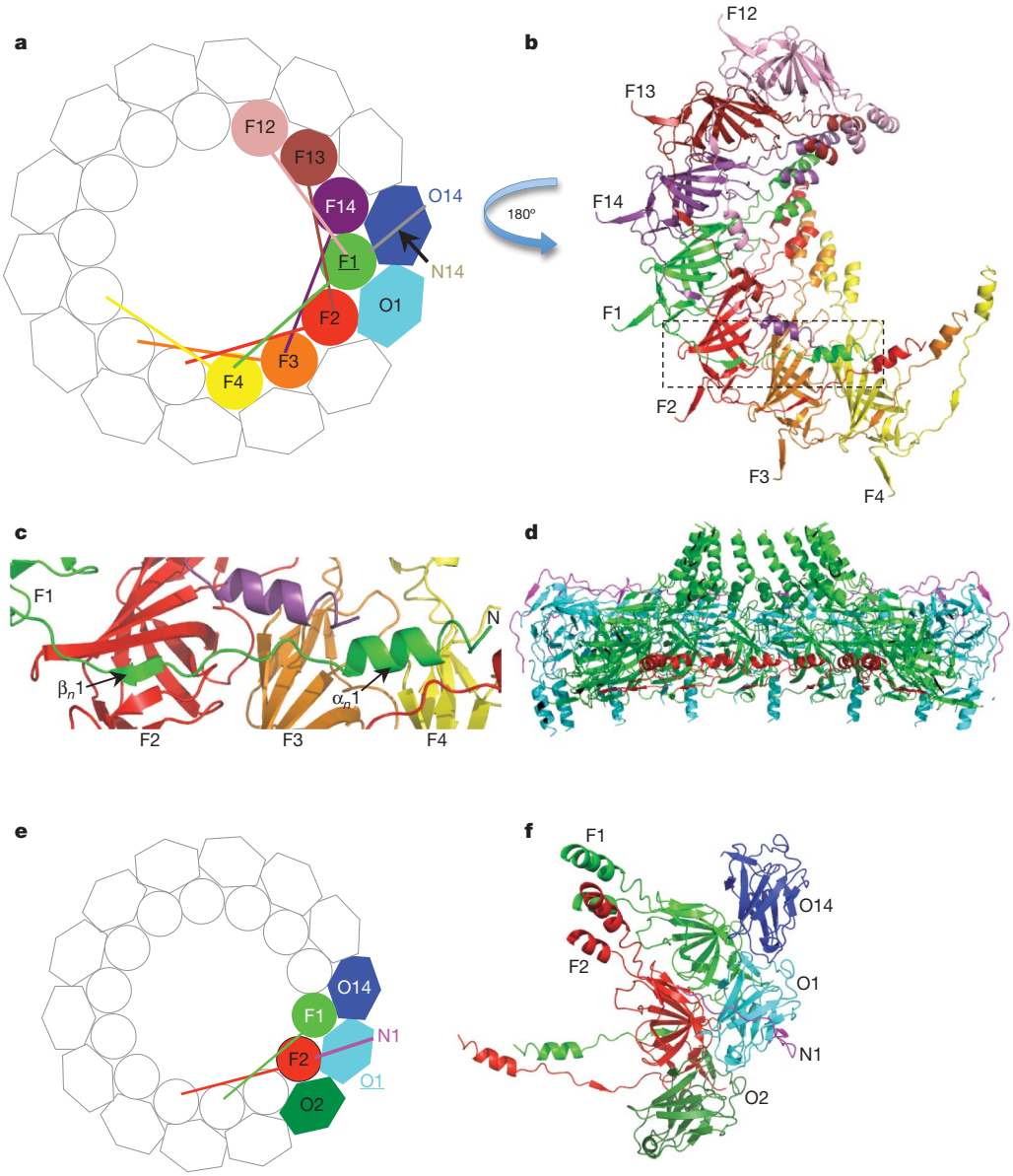

Figure 3 | Inter-heterotrimeric interactions. **a**, Schematic diagram of the tetradecamer with emphasis on interactions with the $TraF_{CT}$ subunit in green (F1). $TraF_{CT}$ and $TraO_{CT}$ subunits are shown in circles and hexagons, respectively. Not shown for clarity: TraN subunits (except N14, which makes interactions with F1) and the lever arms of subunits not interacting with F1. **b**, Ribbon diagram of the F1-interacting $TraF_{CT}$ subunits (that is, F4, F3, F2, F14, F13 and F12) viewed from the periplasm; that is, turned 180° compared with the view in **a**. The rectangle locates the lever arm of subunit F1. **c**, Interactions of subunits F2, F3 and F4 with the lever arm of subunit F1. The secondary structures of the lever arm of F1 are labelled. The F2, F3 and F4 subunits are in ribbon representation and labelled accordingly. **d**, Cut-away side view of the outer-membrane complex with the proteins in ribbon diagram representation colour-coded as in Fig. 1 but for the N-terminal arms of the $TraF_{CT}$ subunits in red. **e**, Schematic diagram of the tetradecamer with emphasis on interactions with the $TraO_{CT}$ subunit in cyan (O1). Not shown for clarity: TraN subunits (except N1, which makes interactions with O1) and the lever arms of subunits not interacting with O1. **f**, Ribbon diagram of the subunits shown in colour at left. This view is from the extracellular milieu.

In the tetradecameric structure of the outer-membrane complex, $TraO_{CT}$ interacts with five proteins: two adjacent $TraO_{CT}$ subunits, 1 $TraF_{CT}$ subunit of an adjacent heterotrimer, 1 $TraF_{CT}$ and 1 TraN within its own heterotrimer (Fig. 3e, f). Overall, 49.25% of the total surface area of $TraO_{CT}$ is involved in protein–protein interaction, 43% of which is with the adjacent heterotrimer proteins (Supplementary Fig. 8c, d). The interfaces between adjacent $TraO_{CT}$ subunits and between $TraO_{CT}$ of one heterotrimer and $TraF_{CT}$ of an adjacent heterotrimer (described in the Supplementary Information and Supplementary Fig. 7) mostly consist of loop residues (Fig. 3f).

The outer-membrane pore

Viewed from the top, the structure contains a central hydrophobic ring of 76 Å in diameter (Fig. 4a, left panel) with a 32 Å pore in the middle. This region consists of a ring of two-helix bundles (Fig. 4a, lower right panel) formed by helices α2 and α3 of the $TraF_{CT}$ antenna. These helices each form a ring, with the α3 ring inside the α2 ring, suggesting that α2 is the transmembrane helix contacting the membrane. Two lines of evidence indicate that this region is inserted in the outer membrane and forms the outer-membrane channel. First, α2, the external helix in the two-helix bundle, has all the features of a transmembrane helix: it is amphipathic, with its hydrophobic side expected to contact the membrane, and is strongly predicted to form a transmembrane helix by TMPred (http://www.ch.embnet.org/software/TMPRED_form.html). Second, when a Flag-tag is inserted between helices α2 and α3 of TraF in the full-length core complex, the tag is found exposed extracellularly (Fig. 4b), demonstrating that the two-helix bundle projects across the outer membrane. Altogether, these results unambiguously assign the two-helix bundle region of TraF/VirB10 as the channel-forming region of T4S systems.

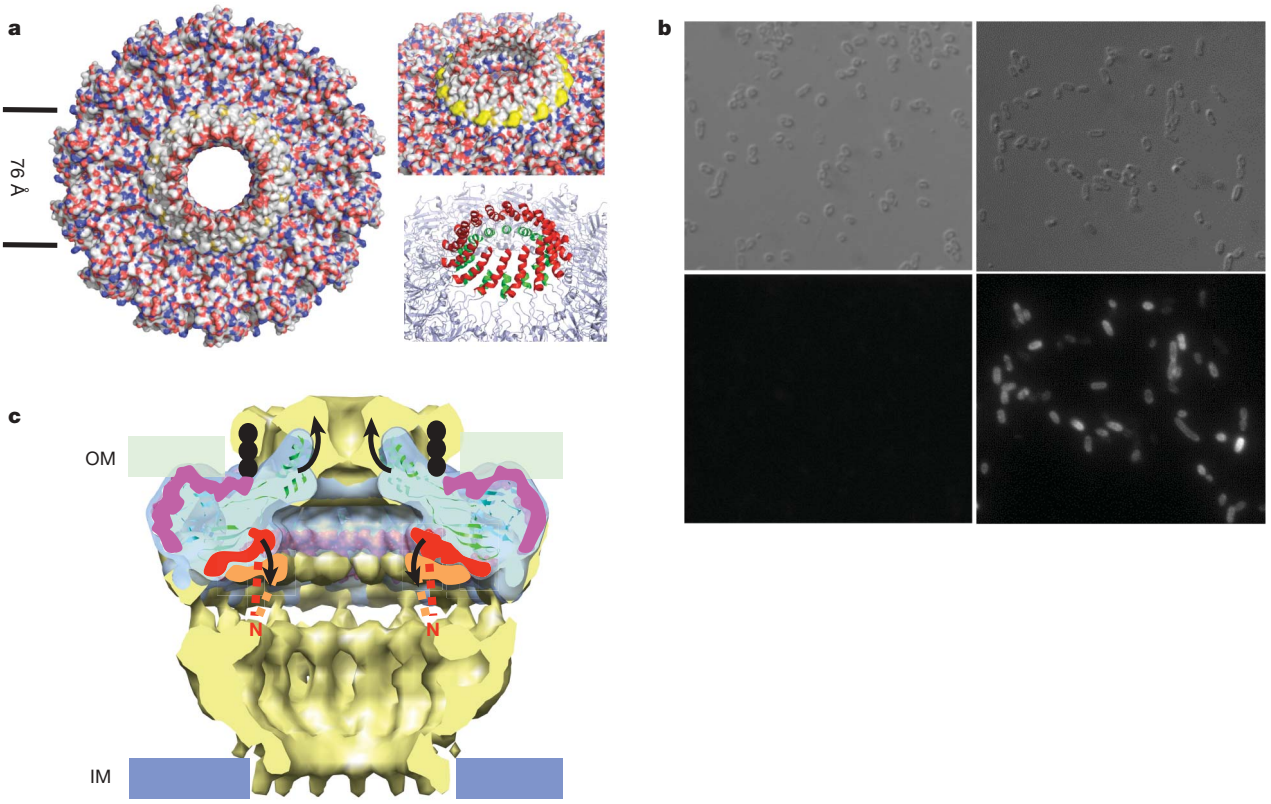

Figure 4 | Transmembrane region of the T4S system outer-membrane complex and proposed mechanism of pore opening and closure. **a**, Left panel: surface diagram of complex viewed from the extracellular milieu. The two lines define the hydrophobic central region around the pore. Top right panel: same as at left but showing (in yellow) the ring of Trp residues at the base of α2. Bottom right panel: ribbon diagram of the transmembrane helices with the internal and external ring of helices colour-coded in green and red, respectively. **b**, Extracellular detection of the Flag-tag located between helices α2 and α3 of TraF. A Flag-tag was introduced in the loop between the α2 and α3 helices of TraF as described in Methods. Upper and lower left panels: control sample expressing the wild-type T4S system core complex. Upper and lower right panels: cells expressing the Flag-tagged T4S system core complex. Differential interference contrast images are shown in the upper panels and the corresponding fluorescence images in the lower panels. **c**, Proposed mechanism for pore opening and closure. The cryo-EM core complex structure (pale yellow) is superimposed on the crystal structure of the outer-membrane complex (pale cyan). The N-terminal lever arm shelf is highlighted in orange and red in the cryo-EM and crystal structures, respectively. The position of the lipid on TraN/VirB7 is indicated in black dots. TraN/VirB7 is shown in magenta. Proposed conformational changes are illustrated by arrows. The N-terminal sequences linking the lever arms to sequences in the I layer are shown in dashed lines colour-coded red and orange for the conformations found in the crystal and cryo-EM structures, respectively. OM, outer membrane; IM, inner membrane.

α-Helical insertions into outer membranes have been observed only once before, in Wza[15,16]. In Wza, the C terminus forms an α-helix and eight of them in the Wza octamer were shown unambiguously to form the outer-membrane channel. The outer-membrane channel of the T4S system differs by forming a two-helix bundle ring system. As in Wza, a tryptophan residue lies at the N-terminal base of the TraF transmembrane helix contacting the membrane (α2; Fig. 4a, upper right panel)[15]. This Trp residue is conserved in most VirB10 protein family members. In the structure presented here, the outer-membrane-inserting region has been cleaved by chymotrypsin (Fig. 1a) and the region around the cleavage is disordered (residues 322–344 could not be traced because of poor electron density). As a result, the transmembrane α2 helices are one turn shorter than those forming the outer-membrane channel of Wza. Another consequence of this structural disorder is that the extent of the opening cannot be precisely defined.

The T4S system outer-membrane complex, in addition to being much larger than previously described outer-membrane structures (for example Wza or TolC), is also radically different in shape (Supplementary Fig. 9): whereas the Wza homo-octamer and the homo-TolC trimer are elongated[15,17], the hetero-tetradecameric T4S system outer-membrane complex spreads out just under the outer membrane, creating a vast contact area with the inner leaflet of the outer membrane. This contact area is mostly mediated by the $TraO_{CT}$–TraN complex ring. In effect, the $TraO_{CT}$–TraN complex ring appears to buttress the entire T4S system against the inner leaflet of the outer membrane, possibly allowing the system to exert much greater mechanical forces to extrude substrates than would otherwise be feasible in systems like Wza or TolC, which make limited contacts with the inner leaflet of the outer membrane.

Conformational changes in T4S systems

The cryo-EM structure of the T4S system core complex revealed a double-walled structure in the cap of the O layer (Supplementary Fig. 10a)[12]. The crystal structure of the cap is not double-walled. This is because the lipid moiety of TraN/VirB7 was not built (the single-wavelength anomalous dispersion (SAD)-derived map showed electron density connecting to Cys 15 of TraN/VirB7 (the lipidation site) but the density was not sufficiently well-defined for unambiguous fitting). However, when the crystal structure of the outer-membrane complex is superimposed on the cryo-EM structure of the entire complex (Fig. 4c), Cys 15 of TraN aligns perfectly at the base of the outer wall of the cap, suggesting that this part of the cap might indeed contain the lipidated part of TraN (indicated in Fig. 4c in black dots).

The superposition of the structure of the outer-membrane complex and that of the core complex (Fig. 4c; such a superposition is valid as one complex is derived from the other by proteolysis) also reveals that the transmembrane helices overlap partly with the first half of the inner wall of the cap, suggesting that they might form this region of the cap. However, the crystal structure captures them in a different conformation than that observed in the cryo-EM structure: whereas in the cryo-EM structure they form a narrow vertical constriction, in the crystal structure they lie in a 'relaxed' state at a 45°

angle. Thus, the two structures may represent different states. Presumably, by removing the entire N-terminal half of TraF, the constraints that this half places on the N-terminal lever arm of $TraF_{CT}$ might have been removed, releasing the lever arms and leading to relaxation of the transmembrane helices. Indeed, as illustrated in Fig. 4c, sequences N-terminal to the α_n1 helix would directly connect to the I layer (schematically shown in Fig. 4c by dashed red lines) and are likely to bring the N-terminal arm of each TraF/VirB10 subunit down. This is consistent with the fact that the shelf formed by the N-terminal lever arms of TraF/VirB10 subunits has shifted up in the crystal structure compared with its position in the cryo-EM structure of the full-length core complex (Fig. 4c and Supplementary Fig. 10a, b in orange and red, respectively). Thus, we propose that the N-terminal arms of the TraF/VirB10 subunits might act in concert to exert conformational changes in the T4S system channel upon signals sensed by the N-terminal domain of the protein (see below).

In *A. tumefaciens*, VirB10 is known to undergo a conformational change induced by the energizing T4S system components[18]. The structure of the T4S system outer-membrane complex reveals that VirB10 forms the outer-membrane channel. However, VirB10 is also known to insert in the inner membrane, making contact not only with the inner-membrane channel component VirB8, but also with the ATPases[13,19,20]. Thus, VirB10 is in a unique position to relay conformational changes taking place in the ATPases and to effect pore opening and closure at the outer membrane. Also, in *A. tumefaciens*, VirB10 does not directly contact the substrate, but regulates its handover from the VirB6/VirB8 complex in the inner membrane to VirB9 and VirB2, the major pilin[21]. As VirB10 lines the interior of the outer-membrane complex, it is difficult to envisage how the substrate could not interact with it, unless it is insulated from the substrate by another layer of protein, presumably made of the VirB2 pilin. We thus propose that the VirB2 pilin forms a cylindrical conduit encased within the VirB10 ring. This hypothesis is also consistent with the observation that, in the state captured in the crystal structure (where VirB2 is absent), the TraF/VirB10 transmembrane helices have somewhat caved in.

The crystal structure of the T4S system outer-membrane complex reveals an outer-membrane structure of unprecedented size and complexity. This structure is held together by a dense network of protein–protein interactions, which provides a rich targeting ground for inhibitor design. Most striking among them is the extensive interaction that the N-terminal lever arms of the $TraF_{CT}$ subunits make with numerous subunits along the tetradecameric structure. We hypothesized that these sequences are at the heart of a nanodevice regulating T4S. If confirmed, this mechanism could become key to the design of inhibitor compounds specifically targeting the T4S machinery.

METHODS SUMMARY

Purification, crystallization, X-ray diffraction data collection. The T4S system core complex was expressed and purified as described previously[12]. After addition of chymotrypsin, the T4S system outer-membrane complex was purified by gel filtration. Crystals were grown by hanging-drop vapour diffusion. Native and SAD data at the selenium edge were collected at the European Synchrotron Radiation Facility beamline ID14.4 and Soleil's beamline PROXIMA 1, respectively, and processed using the XDS package.

Structure determination and refinement. The structure was solved by molecular replacement using the native data set and the known 20 Å resolution cryo-EM map of the trypsin-cleaved core complex as search model[12]. Fourteen-fold non-crystallographic symmetry averaging and phase extension to 2.8 Å resolution yielded a readily interpretable electron density map. This map was used to locate selenium atoms using the SAD data set. These heavy-metal sites were used to generate SAD phases to 2.6 Å resolution, also yielding an interpretable electron density map.

Extracellular localization of a Flag-tag inserted between the α2 and α3 helices of TraF. A Flag-tag was introduced at position 332 in the loop between the α2 and α3 helices of TraF. Cells expressing either the wild-type core complex or the Flag-tagged core complex were grown, fixed and incubated with anti-Flag antibodies followed by goat anti-mouse IgG1 Texas Red antibodies. Fluorescence was monitored using a Zeiss Axioskop microscope, and images collected using a Hamamatsu Orca ER camera.

Full Methods and any associated references are available in the online version of the paper at www.nature.com/nature.

Received 26 June; accepted 19 October 2009.
Published online 29 November 2009.

1. Fronzes, R., Christie, P. J. & Waksman, G. The structural biology of type IV secretion systems. *Nature Rev. Microbiol.* **7,** 703–714 (2009).
2. Christie, P. J., Atmakuri, K., Krishnamoorthy, V., Jakubowski, S. & Cascales, E. Biogenesis, architecture, and function of bacterial type IV secretion systems. *Annu. Rev. Microbiol.* **59,** 451–485 (2005).
3. Schroder, G. & Lanka, E. The mating pair formation system of conjugative plasmids – a versatile secretion machinery for transfer of proteins and DNA. *Plasmid* **54,** 1–25 (2005).
4. Backert, S. & Selbach, M. Role of type IV secretion in *Helicobacter pylori* pathogenesis. *Cell. Microbiol.* **10,** 1573–1581 (2008).
5. Ninio, S. & Roy, C. R. Effector proteins translocated by *Legionella pneumophila*: strength in numbers. *Trends Microbiol.* **15,** 372–380 (2007).
6. McCullen, C. A. & Binns, A. N. *Agrobacterium tumefaciens* and plant cell interactions and activities required for interkingdom macromolecular transfer. *Annu. Rev. Cell Dev. Biol.* **22,** 101–127 (2006).
7. Burns, D. L. Type IV transporters of pathogenic bacteria. *Curr. Opin. Microbiol.* **6,** 29–34 (2003).
8. Thomas, C. M. & Nielsen, K. M. Mechanisms of, and barriers to, horizontal gene transfer between bacteria. *Nature Rev. Microbiol.* **3,** 711–721 (2005).
9. Fronzes, R., Remaut, H. & Waksman, G. Architectures and biogenesis of non-flagellar protein appendages in Gram-negative bacteria. *EMBO J.* **27,** 2271–2280 (2008).
10. Gomis-Ruth, F. X. & Coll, M. Cut and move: protein machinery for DNA processing in bacterial conjugation. *Curr. Opin. Struct. Biol.* **16,** 744–752 (2006).
11. Bayliss, R. *et al.* NMR structure of a complex between the VirB9/VirB7 interaction domains of the pKM101 type IV secretion system. *Proc. Natl Acad. Sci. USA* **104,** 1673–1678 (2007).
12. Fronzes, R. *et al.* Structure of a type IV secretion system core complex. *Science* **323,** 266–268 (2009).
13. Jakubowski, S. J. *et al. Agrobacterium* VirB10 domain requirements for type IV secretion and T pilus biogenesis. *Mol. Microbiol.* **71,** 779–794 (2009).
14. Terradot, L. *et al.* Structures of two core subunits of the bacterial type IV secretion system, VirB8 from *Brucella suis* and ComB10 from *Helicobacter pylori*. *Proc. Natl Acad. Sci. USA* **102,** 4596–4601 (2005).
15. Dong, C. *et al.* Wza the translocon for *E. coli* capsular polysaccharides defines a new class of membrane protein. *Nature* **444,** 226–229 (2006).
16. Meng, G., Fronzes, R., Chandran, V., Remaut, H. & Waksman, G. Protein oligomerization in the bacterial outer membrane. *Mol. Membr. Biol.* **26,** 136–145 (2009).
17. Koronakis, V., Sharff, A., Koronakis, E., Luisi, B. & Hughes, C. Crystal structure of the bacterial membrane protein TolC central to multidrug efflux and protein export. *Nature* **405,** 914–919 (2000).
18. Cascales, E. & Christie, P. J. *Agrobacterium* VirB10, an ATP energy sensor required for type IV secretion. *Proc. Natl Acad. Sci. USA* **101,** 17228–17233 (2004).
19. Atmakuri, K., Cascales, E. & Christie, P. J. Energetic components VirD4, VirB11 and VirB4 mediate early DNA transfer reactions required for bacterial type IV secretion. *Mol. Microbiol.* **54,** 1199–1211 (2004).
20. Llosa, M., Zunzunegui, S. & de la Cruz, F. Conjugative coupling proteins interact with cognate and heterologous VirB10-like proteins while exhibiting specificity for cognate relaxosomes. *Proc. Natl Acad. Sci. USA* **100,** 10465–10470 (2003).
21. Cascales, E. & Christie, P. J. Definition of a bacterial type IV secretion pathway for a DNA substrate. *Science* **304,** 1170–1173 (2004).

Supplementary Information is linked to the online version of the paper at www.nature.com/nature.

Acknowledgements This work was funded by Wellcome Trust grant 082227 to G.W. We thank A. Thompson and the staff of beamline PROXIMA 1 at Soleil, the staff of beamline ID14.4 at the European Synchrotron Radiation Facility, and H. Saibil, E. Orlova and P. Christie for comments on the manuscript. We thank A. Kumar for help in implementing the immunofluorescence experiments.

Author Contributions V.C. produced the complex, optimized crystals, and built, refined and analysed the structure. R.F. designed the purification protocol, produced the complex, grew the first crystals, optimized crystals and analysed the structure. S.D. and J.N. solved the structure by molecular replacement and provided the electron density map. N.C. collected crystallographic data. G.W. supervised the work, analysed the structure and wrote the paper.

Author Information Structure factors and coordinates are deposited in the Protein Data Bank under accession number 3JQO. Reprints and permissions information is available at www.nature.com/reprints. Correspondence and requests for materials should be addressed to G.W. (g.waksman@ucl.ac.uk or g.waksman@bbk.ac.uk).

METHODS

Purification of the outer-membrane complex. Expression of the T4S system core complex from the IBA3c:*traN-traF*$_{C\text{-}ST}$ plasmid was induced using 200 μg l^{-1} of anhydrotetracyclin[12]. After incubation overnight at 16 °C, the complex was extracted from the membrane fraction and purified using a Strep-Tactin sepharose affinity column (IBA) as described previously[12]. The elution fractions containing the core complex were pooled together and subjected to limited proteolysis with 2 mg ml^{-1} of chymotrypsin for 3 h at room temperature. The proteolysed sample was then concentrated using a 100-kDa cut-off spin concentrator (Amicon) and loaded onto a Superose 6 GL 10/300 (GE Healthcare) gel filtration column in 50 mM TrisHCl pH 8.0, 200 mM NaCl and 10 mM LDAO. The outer-membrane complex eluted as a single peak (Supplementary Fig. 1a).

Selenomethionine labelling. The IBA3c:*traN-traF*$_{C\text{-}ST}$ plasmid[12] was transformed into B834(DE3) competent cells (Novagen). Expression of the selenomethionine (SeMet)-labelled proteins was performed at 16 °C overnight in M9 minimal medium supplemented with 50 mg l^{-1} of SeMet. Purification of the SeMet-labelled outer-membrane complex was as described above for the native complex.

Crystallization and data collection. Large rod-like crystals were grown by vapour diffusion method at 20 °C using hanging drops containing 15 mg ml^{-1} of the purified native and SeMet-labelled complexes and 20–40% w/v MPD, 100 mM Bis-Tris pH 6.5–7.5. The crystals were flash frozen in liquid nitrogen using the mother liquor as the cryoprotectant. For the SeMet crystals, the oxidation protocol described in Sharff *et al.*[22] was used before crystallization. The oxidized SeMet crystals were further flash-soaked in 0.1% H_2O_2 in 50% w/v MPD, 100 mM Bis-Tris, pH 7.0 before flash freezing for data collection. Data collection was performed at the beamline ID14-4 at European Synchrotron Radiation Facility (Grenoble, France) for the native data set and at beamline PROXIMA 1 at the Soleil Synchrotron (Gif sur Yvette, France) for the oxidized SeMet SAD data set. Data reduction was performed using the XDS package[23]. Data collection statistics are presented in Supplementary Table 1.

Structure determination. The structure was solved by molecular replacement using the native data set and the known 20 Å resolution cryo-EM map of the trypsin-cleaved core complex as search model (Supplementary Fig. 1b)[12]. The orientation and position of the particle was determined using AMoRe[24]. The 35–20 Å resolution range was used and yielded a molecular replacement solution with a correlation coefficient of 0.39. Fourteenfold non-crystallographic symmetry averaging with RAVE, MAMA and other programs of the Uppsala suite[25–27], in combination with the CCP4 suite[28], was used for phase extension to 2.8 Å resolution using the native data set. This yielded a readily interpretable map with well-defined side chains (Supplementary Fig. 1c and Supplementary Table 1). The three component proteins $TraF_{CT}$, $TraO_{CT}$ and TraN were traced manually with the program Coot[29]. Subsequently, this structure was used to locate the selenium atoms in a SAD data set collected to 2.6 Å resolution. Refinement of these sites and phasing (PHASER[30]), followed by density modification exploiting the 14-fold non-crystallographic symmetry in PARROT[28], yielded a readily interpretable electron density map. After initial tracing by BUCCANEER[28], the partial model was used for subsequent cycles of PHASER, PARROT and BUCCANNEER. Further restrained refinement with REFMAC[31] and PHENIX[32,33] was performed using tight restraints on non-crystallographic symmetry throughout the refinement. Final stages of refinement with the map from the SAD data set showed a density for a modified cysteine in the lipoprotein TraN with small disordered lipid chains attached. However, as the density was not good enough for unambiguous building, we refrained from modelling this modification in the final model. The final model has 94.8% residues in the most favoured region, 4.7% residues in the additionally allowed regions and 0.5% residues in the disallowed region of the Ramachandran plot. Refinement statistics are presented in the Supplementary Table 1.

Extracellular localization of a Flag-tag inserted between the α2 and α3 helices of TraF. The Flag epitope was introduced by PCR at position 332 of TraF/VirB10 in the IBA3c:*traN-traF*$_{C\text{-}ST}$ plasmid[12], yielding IBA3c:*traN-traF*$_{Flag,C\text{-}ST}$. The primer sequences were: 5′-GACGACGACAAGATTCAGTACAACAGCACAGAA-3′ (forward) and 5′-GTCCTTGTAGTCGTTATTACTCTGCGTCTGGTT-3′ (reverse). Expression and purification of the resulting Flag-tagged T4S system core complex yielded a complex very similar in molecular mass to the wild-type complex (1.05 MDa), indicating that the Flag-tag does not disturb core complex assembly. *Escherichia coli* TOP10 cells containing either the IBA3c:*traN-traF*$_{C\text{-}ST}$ plasmid (the expression of which results in the production of the wild-type T4S system core complex)[12] or the IBA3c:*traN-traF*$_{Flag,C\text{-}ST}$ plasmid (the expression of which results in the production of the T4S system core complex containing a Flag-tag at position 332 of TraF) were grown at 37 °C to an optical density ($OD_{600\,nm}$) of 0.6. Protein expression was induced by addition of 200 μg l^{-1} of anhydrotetracyclin and cells were incubated at 16 °C overnight. Cells were collected by centrifugation, resuspended in ice-cold 4% formaldehyde and incubated on ice for 15 min. The fixed cells were washed twice with PBS and re-suspended in PBS. The cell suspensions were applied to poly-L-lysine-treated microscope slides and incubated at room temperature for 20 min. The slides were rinsed in PBS and blocked in 1% goat serum-PBS for 45 min. The primary antibody (anti-Flag M2 Mab (Sigma), 1:1,000 dilution) was applied and incubated on the slide at 4 °C overnight. The slides were washed twice with PBS at room temperature and the secondary antibody (goat anti-mouse IgG1 Texas Red (Southern Biotech), 1:500 dilution) was applied and incubated on the slide for 1 h. The slides were then washed twice with PBS and were mounted using DAKO fluorescent mounting medium. The fluorescence microscopy was performed on a Zeiss Axioskop microscope, objective ×100 with oil. The images were collected using a Hamamatsu Orca ER camera.

22. Sharff, A. J., Koronakis, E., Luisi, B. & Koronakis, V. Oxidation of selenomethionine: some MADness in the method! *Acta Crystallogr. D* **56,** 785–788 (2000).
23. Kabsch, W. Automatic processing of rotation diffraction data from crystals of initially unknown symmetry and cell constants. *J. Appl. Cryst.* **26,** 795–800 (1993).
24. Navaza, J. AMoRe: an automated package for molecular replacement. *Acta Crystallogr. A* **50,** 157–163 (1994).
25. Jones, T. A. in *Molecular Replacement* 91–95 (CCP4 Proceedings, 1992) ⟨http://epubs.cclrc.ac.uk/bitstream/948/DL-SCI-R33.pdf⟩.
26. Kjeldgaard, M. & Jones, T. A. in *From First Map to Final Model* 59–66 (CCP4 Proceedings, 1994) ⟨http://epubs.cclrc.ac.uk/bitstream/950/DL-SCI-R35.pdf⟩.
27. Kleywegt, G. & Jones, T. Software for handling macromolecular envelopes. *Acta Crystallogr. D* **55,** 941–944 (1999).
28. Collaborative Computational Project, Number 4. The *CCP*4 suite: programs for protein crystallography. *Acta Crystallogr. D* **50,** 760–763 (1994).
29. Emsley, P. & Cowtan, K. Coot: model-building tools for molecular graphics. *Acta Crystallogr. D* **60,** 2126–2132 (2004).
30. McCoy, A. *et al.* Phaser crystallographic software. *J. Appl. Cryst.* **40,** 658–674 (2007).
31. Murshudov, G., Vagin, A. & Dodson, E. Refinement of macromolecular structures by the maximum-likelihood method. *Acta Crystallogr. D* **53,** 240–255 (1997).
32. Adams, P. D. *et al.* PHENIX: building new software for automated crystallographic structure determination. *Acta Crystallogr. D* **58,** 1948–1954 (2002).
33. Afonine, P. V., Grosse-Kunstleve, R. W. & Adams, P. D. The Phenix refinement framework. *CCP4 Newsl.* 42, contribution 8 (2005) ⟨http://www.ccp4.ac.uk/newsletters/newsletter42.pdf⟩.